Conformational Dynamics and Proton Relay Positioning in Nickel Catalysts for Hydrogen Production and Oxidation

ARTICLE *in* ORGANOMETALLICS · DECEMBER 2013

Impact Factor: 4.13 · DOI: 10.1021/om400695w

11 AUTHORS, INCLUDING:

Ming-Hsun Ho
Pacific Northwest National Laboratory
22 PUBLICATIONS **325** CITATIONS
SEE PROFILE

Tianbiao Liu
Pacific Northwest National Laboratory
40 PUBLICATIONS **956** CITATIONS
SEE PROFILE

Simone Raugei
Pacific Northwest National Laboratory
96 PUBLICATIONS **1,742** CITATIONS
SEE PROFILE

ORGANOMETALLICS

Article

pubs.acs.org/Organometallics

Conformational Dynamics and Proton Relay Positioning in Nickel Catalysts for Hydrogen Production and Oxidation

James A. Franz, Molly O'Hagan, Ming-Hsun Ho, Tianbiao Liu, Monte L. Helm, Sheri Lense, Daniel L. DuBois, Wendy J. Shaw, Aaron M. Appel,* Simone Raugei,* and R. Morris Bullock

Center for Molecular Electrocatalysis, Pacific Northwest National Laboratory, P.O. Box 999, K2-57, Richland, Washington 99352, United States

Supporting Information

ABSTRACT: The $[Ni(P^R_2N^{R'}_2)_2]^{2+}$ complexes (where $P^R_2N^{R'}_2$ is 1,5-R′-3,7-R-1,5-diaza-3,7-diphosphacyclooctane) are fast electrocatalysts for H_2 production and oxidation. Binding of a fifth ligand (CH_3CN or BF_4^-) or chair/boat isomerization has the potential to slow catalysis by blocking the addition of H_2 or by incorrectly positioning the pendant amines. We report the structural dynamics of a series of nickel complexes characterized by NMR spectroscopy and theoretical modeling to examine the effects of the fifth ligand for the Ni(II) complexes, including CH_3CN, BF_4^-, Cl^-, and H^-, as well as the differences in dynamics between the Ni(II) and Ni(0) oxidation states. A fast exchange process was observed for the $[Ni(CH_3CN)(P^R_2N^{R'}_2)_2]^{2+}$ complexes, with rates ranging from 10^4 to 10^7 s^{-1} depending on the phosphorus and nitrogen substituents on the $P^R_2N^{R'}_2$ ligand. This exchange process was identified to occur through a multistep mechanism, which consists of dissociation of the acetonitrile, boat/chair isomerization of each of the four rings (including nitrogen inversion), and reassociation of an acetonitrile on the opposite side of the complex. The rate of the chair/boat inversion was found to be influenced by varying the substituent on the nitrogen atom, but the rate of the overall exchange process is at least an order of magnitude faster than the catalytic rate in acetonitrile, demonstrating that the structural dynamics of the $[Ni(CH_3CN)(P^R_2N^{R'}_2)_2]^{2+}$ complexes do not hinder catalysis. Possible catalytic implications of the coordination of a fifth ligand to the Ni(II) complex are discussed.

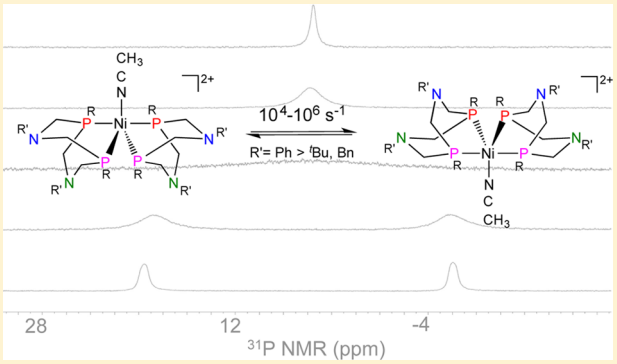

INTRODUCTION

The widespread and efficient use of intermittent power sources, such as solar and wind, will be aided by the development of electrocatalysts that interconvert electricity and fuels for energy storage. One of the focuses of our laboratory is developing an understanding of how to design electrocatalysts that interconvert electricity and H_2 fuel, utilizing pendant amine ligand motifs inspired by the [FeFe]-hydrogenase active site.[1] In these systems, understanding the intricate details of ligand movement and how it affects catalytic efficiencies is an important aspect of designing improved catalysts. Ligand structural fluctuations can influence substrate binding and product elimination as well as the redox properties of electrocatalysts.

In the $[Ni(P^R_2N^{R'}_2)_2]^{2+}$ family of hydrogen production and oxidation catalysts (Figure 1, where $P^R_2N^{R'}_2$ is 1,5-R′-3,7-R-1,5-diaza-3,7-diphosphacyclooctane), pendant amines in the second coordination sphere act as proton relays, shuttling protons to and from the metal center, thereby enhancing catalysis.[2,3] Incorporating these pendant amines and optimizing their positioning relative to the metal center has led to the design of fast synthetic molecular catalysts for both hydrogen production[3] and oxidation.[4,5] The positioning of the pendant amine is achieved through steric repulsion of the two six-membered rings containing the pendant amines, favoring the conformation in which one ring is in a chair conformation, with the N atom oriented away from the metal, and the other ring is in a boat conformation, with the N atom oriented toward the metal center in an endo position.[6] This endo positioning facilitates interactions between H^+ and H^- on the amine and the metal center, respectively, for H−H bond formation (or the reverse reaction, H_2 cleavage), as illustrated in Figure 1.

While the incorporated amines are usually depicted as static, the observed conformations of the six-membered rings containing the pendant amines are fluxional and undergo isomerization between the chair and boat conformations, as expected for any six-membered ring. The rate of interconversion of the chair and boat isomers may be critical to the rate of proton delivery to/from the metal center.[7,8] The flexibility of

Received: July 15, 2013
Published: November 15, 2013

   dx.doi.org/10.1021/om400695w | Organometallics 2013, 32, 7034−7042

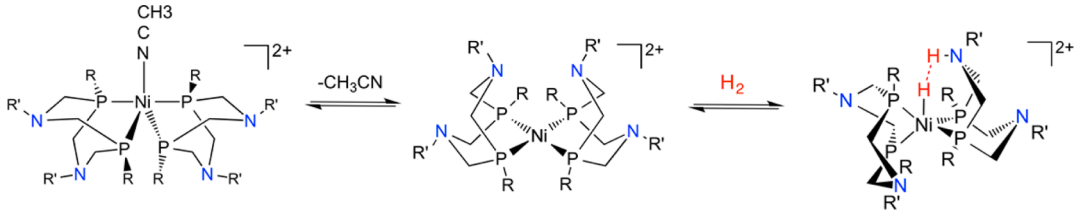

Figure 1. Dissociation of acetonitrile and binding of H_2 in the oxidation of hydrogen (left to right) or the reverse reactions in the production of hydrogen (right to left). The heterolytic cleavage or formation of the H−H bond requires the positioning of a pendant amine endo to the metal center, which is governed by the boat/chair isomerization of the six-membered rings $(Ni(P)_2(C_2)_2N)$.

the six-membered rings and, therefore, the transient nature of the positioned proton relay have not been investigated, and it is unknown whether the rate of interconversion of the various conformers influences the observed catalytic rates.

The propensity of the Ni(II) complex to bind a fifth ligand may also affect the observed catalytic rates. Many Ni(II) complexes of this family have been shown to bind a fifth ligand (CH_3CN, BF_4^-, or Cl^-), at least in the solid state,[9,10] to make a trigonal-bipyramidal complex. For the five-coordinate complexes, such as $[Ni(CH_3CN)(P^R{}_2N^{R'}{}_2)_2]^{2+}$, the dissociation of the fifth ligand is a necessary step to enter the catalytic pathway for hydrogen oxidation and may influence the hydrogen dissociation step in hydrogen production, as illustrated in Figure 1. The binding of a fifth ligand can also affect the potential of the Ni(II/I) couple,[11−13] and in turn, the strength of this binding can be influenced by the electronic properties of the complex, consistent with previously reported experimental data in which electron-withdrawing or electron-donating substituents were incorporated.[9] In most cases for the $[Ni(P^R{}_2N^{R'}{}_2)_2]^{2+}$ systems, the catalytic rates have been measured in acetonitrile; therefore, the binding of acetonitrile may be affecting the observed rates and overpotentials.[3,9,10,14]

^1H and ^{31}P NMR spectroscopy and computational studies have been employed to investigate the effect that structural dynamics might have on the catalytic rates of these $[Ni(P^R{}_2N^{R'}{}_2)_2]^{2+}$ complexes. The specific variables studied include the coordination of different fifth ligands to the Ni(II) complexes, the pendant amine positioning in various oxidation states, and what effect the R and R′ groups have on these processes.

RESULTS AND DISCUSSION

Dynamics Observed for $[Ni(P^R{}_2N^{R'}{}_2)_2]^{2+}$ Complexes and the Role of the Fifth Ligand. At room temperature in acetonitrile, ligand structural dynamics for $[Ni(CH_3CN)(P^R{}_2N^{R'}{}_2)_2]^{2+}$ are evidenced by the broad ^{31}P resonance at approximately +6 ppm, which resolves into two resonances at reduced temperature. As an example, the variable-temperature ^{31}P NMR spectra for $[Ni(CH_3CN)(P^{Ph}{}_2N^{Ph}{}_2)_2]^{2+}$ are shown at the top of Figure 2. The two inequivalent ^{31}P environments are assigned as the axial and equatorial positions of the trigonal-bipyramidal geometry resulting from the coordination of a fifth ligand, as observed in the solid-state structures, in which acetonitrile is coordinated in an equatorial position.[9,10,15] For the NMR spectroscopy experiments performed in the presence of acetonitrile, the fifth ligand is presumed to be acetonitrile but could also potentially be a counteranion such as BF_4^-, which has been observed as a weakly bound fifth ligand in previously reported solid-state structures.[9] Activation parameters were determined using line shape analysis assuming a two-site model

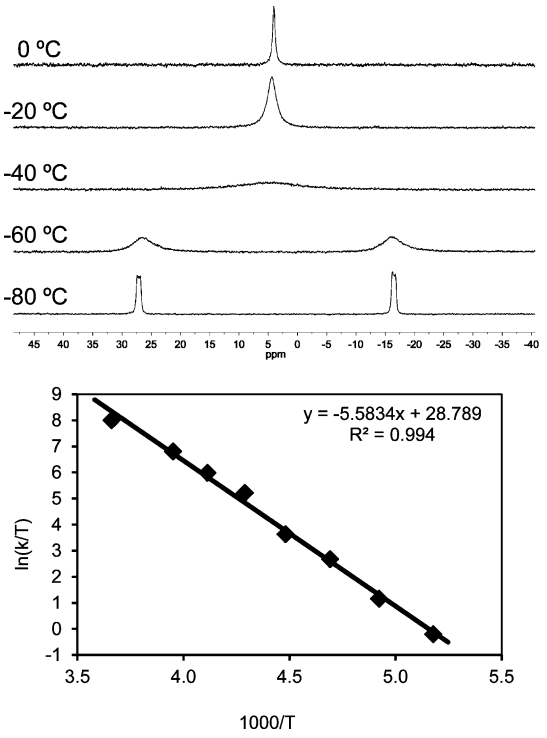

Figure 2. (top) Variable-temperature $^{31}P\{^1H\}$ NMR spectra of $[Ni(CH_3CN)(P^{Ph}{}_2N^{Ph}{}_2)_2]^{2+}$. (bottom) Eyring plot from exchange rates obtained by line shape analysis.

of exchange with gNMR software (see Figures S1 and S2 in the Supporting Information for representative spectra and simulations).[16−18] The Eyring plot of the variable-temperature data over the temperature range of −80 to 20 °C is shown at the bottom of Figure 2. On the basis of the activation parameters derived from this Eyring analysis (Table 1), the rate of ^{31}P exchange is calculated to be 7×10^6 s^{-1} at 25 °C; $\Delta G^{\ddagger} = 8.2$ kcal/mol.

The interconversion between the axial and equatorial ^{31}P nuclei could be the result of either a Berry pseudorotation[19] or the dissociation of the fifth ligand and reassociation after ^{31}P interconversion. To distinguish between these possible exchange processes, $[Ni(Cl)(P^{Ph}{}_2N^{Ph}{}_2)_2]^+$ was synthesized to introduce a fifth ligand that is nonlabile at room temperature. The ^{31}P spectrum, shown in Figure 3, shows no observable fluxional behavior, on the basis of the two distinct ^{31}P resonances observed, which have a complex AA′BB′ coupling pattern. If the fluxional behavior observed in the $[Ni(CH_3CN)(P^{Ph}{}_2N^{Ph}{}_2)_2]^{2+}$ complex is due to Berry pseudorotation, exchange would still be expected to occur with the chloride as the fifth ligand in place of the more labile ligand. The lack of observable exchange in the presence of a coordinated chloride

dx.doi.org/10.1021/om400695w | Organometallics 2013, 32, 7034−7042

Table 1. Rates and Activation Parameters for ^{31}P Exchange in $[Ni(L)(P^{R}_{2}N^{R'}_{2})_2]^{2+}$ Complexes in CD_2Cl_2[a]

R,R′	$rate_{298\ K}$ (s^{-1})	$\Delta H^{\ddagger}$ (kcal/mol)	$\Delta S^{\ddagger}$ (cal/(mol K))	$\Delta G^{\ddagger}_{298\ K}$ (kcal/mol)
Ph,Ph, no CH_3CN	6.5×10^6	8.3 ± 1.4	0.3 ± 1.8	8.2
Ph,Ph, 20% CH_3CN	7.0×10^6	11 ± 2.0	9.3 ± 2.0	8.2
Cy,Ph, 20% CH_3CN	1.8×10^7	10 ± 1.6	7.3 ± 1.6	7.9
Ph,^{t}Bu, no CH_3CN	4.5×10^4	9.5 ± 1.6	−5.0 ± 1.8	11.0
Ph,^{t}Bu, 20% CH_3CN	3.1×10^4	9.0 ± 1.4	−3.1 ± 1.9	10.0

[a] L = CH_3CN, BF_4^-. Errors are reported as two standard deviations.

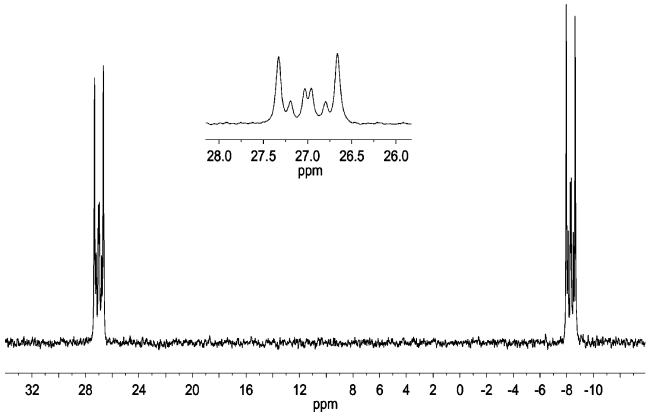

Figure 3. $^{31}P\{^1H\}$ NMR spectrum of $[Ni(Cl)(P^{Ph}_{2}N^{Ph}_{2})_2]^+$ at 25 °C in CD_3CN. The two distinct resonances suggest that the nonlabile fifth ligand hinders the structural dynamics. The inset shows the AA′BB′ coupling pattern in an expansion of the 26−28 ppm region.

suggests that the exchange process requires a labile fifth ligand such as acetonitrile and therefore is not Berry pseudorotation.

Because of the lack of exchange in the $[Ni(Cl)(P^{Ph}_{2}N^{Ph}_{2})_2]^+$ complex, full NMR resonance assignments were possible using 2D NMR techniques, including COSY, TOCSY, HSQC, and HMBC. See Figures S3 and S4 and Table S1 (Supporting Information) for representative $^1H-^{13}C$ HSQC, X-ray structure, and a full summary of resonance assignments.

To investigate whether the observed exchange process involved acetonitrile coordination, the variable-temperature NMR studies were repeated in CD_2Cl_2 without acetonitrile. Under these conditions, a dynamic behavior similar to that seen in the presence of acetonitrile was observed, as shown at the top of Figure 4. The chemical shifts of the two distinct ^{31}P resonances are shifted from 27 to 20 ppm and from −17 to −7 ppm when no acetonitrile is present, although similar ^{31}P NMR exchange rates are observed (6.4×10^6 s^{-1} at 25 °C, with activation parameters reported in Table 1; the Eyring plot in given in Figure S5 (Supporting Information)).

The solid state structure of the complex in the absence of acetonitrile (Figure 4, bottom) revealed that the BF_4^- counterion is bound to the metal in the fifth coordination site. The Ni···F1 distance is 2.969 Å, and the B−F1 distance (1.418(3) Å) is elongated in comparison to the other B−F distances, which range from 1.371 to 1.382 Å, consistent with fluorine coordination,[20,21] as observed previously in the solid state in the absence of CH_3CN.[9] The observation of the coordinated BF_4^- suggests that the exchange process observed

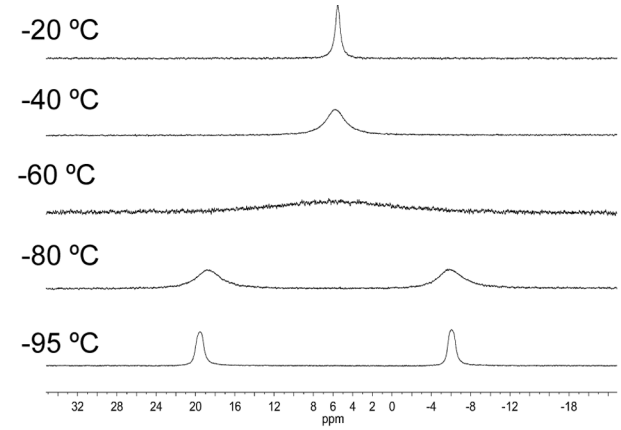

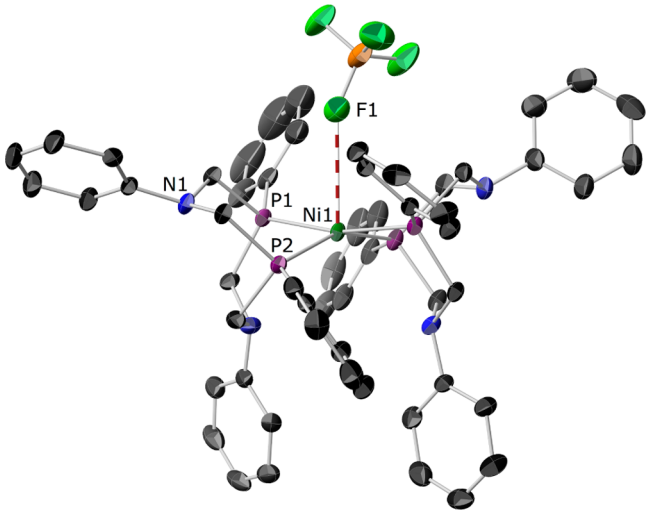

Figure 4. (top) Variable-temperature $^{31}P\{^1H\}$ NMR spectra of $[Ni(BF_4)(P^{Ph}_{2}N^{Ph}_{2})_2]^+$ in CD_2Cl_2 in the absence of acetonitrile. (bottom) Molecular structure of $[Ni(BF_4)(P^{Ph}_{2}N^{Ph}_{2})_2]^+$ showing weakly coordinated BF_4^- as the fifth ligand. Thermal ellipsoids are shown at 30% probability. Hydrogen atoms and the noncoordinated BF_4^- anion are omitted for clarity. Color scheme: gray, carbon; green, fluorine; purple, phosphorus; blue, nitrogen; orange, boron; dark green, nickel.

in the ^{31}P NMR spectra is still dependent upon the fifth ligand, though in this case the BF_4^- anion is the fifth ligand rather than acetonitrile. Similar dynamic behavior is also observed for $[Ni(BF_4)(P^{Ph}_{2}N^{tBu}_{2})_2]^+$, with and without CH_3CN (Table 1). However, a different dynamic behavior is observed when the phenyl substituent on the P atoms is replaced by a cyclohexyl group. When acetonitrile is added to $[Ni(P^{Cy}_{2}N^{Ph}_{2})_2]^{2+}$, the ^{31}P nuclei become inequivalent (Figure 5B) and undergo an exchange process similar to that observed for the $[Ni(P^{Ph}_{2}N^{Ph}_{2})_2]^{2+}$ and $[Ni(P^{Ph}_{2}N^{tBu}_{2})_2]^{2+}$ complexes, which are compared in Table 1. However, when acetonitrile is removed from the $[Ni(P^{Cy}_{2}N^{Ph}_{2})_2]^{2+}$ complex, only a single peak for the ^{31}P nuclei is observed in the absence of acetonitrile at low temperature (Figure 5A), consistent with a single ^{31}P environment. The absence of the exchange process without acetonitrile suggests that the complex with cyclohexyl substituents at phosphorus does not bind BF_4^- as strongly in solution as the analogous complexes with phenyl substituents at phosphorus, presumably due to the difference in the steric and electronic properties of the cyclohexyl substituents. The

dx.doi.org/10.1021/om400695w | Organometallics 2013, 32, 7034−7042

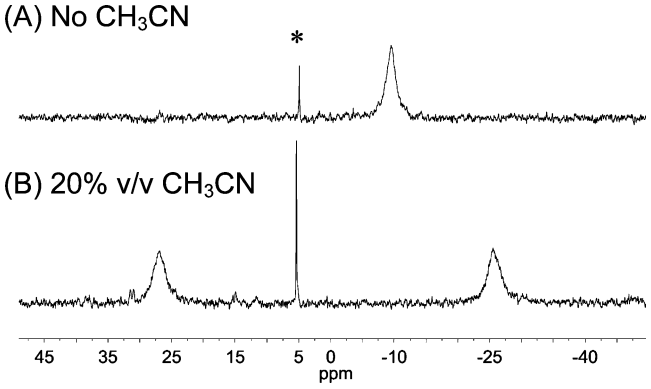

Figure 5. $^{31}P\{^{1}H\}$ NMR spectra of $[Ni(P^{Cy}{}_2N^{Ph}{}_2)_2]^{2+}$ at −80 °C in CD_2Cl_2 (A) with no acetonitrile and (B) with 20% v/v acetonitrile to form $[Ni(CH_3CN)(P^{Cy}{}_2N^{Ph}{}_2)_2]^{2+}$. The asteisk denotes an unidentified impurity (6%).

dependence of the observed dynamic behavior on the presence of a fifth ligand supports the proposed mechanism that dissociation of the fifth ligand is essential for the axial/equatorial interconversion of the ^{31}P nuclei in these nickel complexes.

Chair/Boat Isomerization. In addition to the dynamics involving the fifth ligand, the ^{1}H NMR spectra of $[Ni(CH_3CN)(P^{Ph}{}_2N^{Ph}{}_2)_2]^{2+}$ or $[Ni(BF_4)(P^{Ph}{}_2N^{Ph}{}_2)_2]^{+}$ showed complex dynamic behavior of the methylene protons and the nitrogen substituents, suggesting that chair/boat isomerization, including inversion of the nitrogen, was occurring over this temperature range. Because of the spectral complexity in this region, it was unclear if the ring isomerization was occurring at the same rate as the axial/equatorial ^{31}P interconversion and therefore whether these two exchange processes were occurring as part of the same overall process. To better compare the rates of these two processes, the $[Ni(CH_3CN)(P^{Ph}{}_2N^{tBu}{}_2)_2]^{2+}$ complex was synthesized, because the interconversion of the chair and boat ring conformers would be observable from the distinct ^{t}Bu resonances. The variable-temperature ^{31}P and ^{1}H NMR spectra were recorded, and exchange rates are shown in Table 2. In the ^{1}H NMR spectra (Figure S6, Supporting Information) the two distinct ^{t}Bu resonances coalesced, indicating interconversion of the chair and boat isomers. The resonances of the methylene and phenyl groups also indicate exchange, consistent with this interpretation. The exchange between the two ^{t}Bu environments was found to occur at rates equivalent to those for the exchange of the ^{31}P nuclei, suggesting that the overall process observed involves both chair/boat isomerization and the exchange of the two phosphines between the axial and equatorial positions. On the basis of the exchange observed by the ^{31}P NMR spectra, the rate of exchange for this process is 4×10^4 s^{-1} at 25 °C.

Table 2. Rates of Exchange at Variable Temperatures for the $[Ni(CH_3CN)(P^{Ph}{}_2N^{tBu}{}_2)_2]^{2+}$ Complex in CD_2Cl_2 with 20% (v/v) CD_3CN

	rate (s^{-1})	
temp (°C)	^{1}H NMR spectra	^{31}P NMR spectra
−65	37	42
−55	81	103
−45	201	265
−35	498	509

Exchange Mechanism. Taken collectively, the ^{31}P and ^{1}H NMR spectroscopy data allow us to propose the following mechanism for the observed exchange process: the loss of the fifth ligand occurs first, followed by isomerization of the six-membered rings including inversion of the nitrogen geometry, then reassociation of a fifth ligand in the opposite position from which the fifth ligand was initially bound. This exchange process is shown in Figure 6. Dissociation of the fifth ligand is presumed to precede ring inversion due to steric crowding, but the exact order cannot be determined from the NMR analysis. Specifically, the net exchange of the two species on the left side of Figure 6 is observed, but the individual steps are not directly observed.

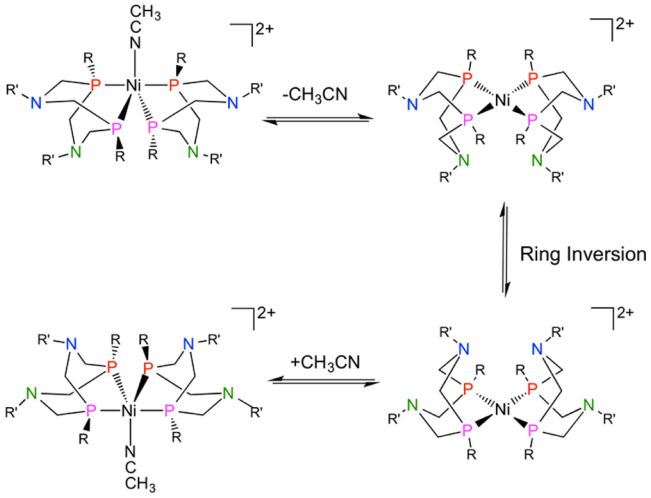

Figure 6. Proposed mechanism of dynamics of $[Ni(CH_3CN)(P^{R}{}_2N^{R'}{}_2)_2]^{2+}$.

The mechanism outlined in Figure 6 is supported and elaborated by a comprehensive computational investigation on $[Ni(CH_3CN)(P^{Ph}{}_2N^{Ph}{}_2)_2]^{2+}$. The dissociation and association of the fifth ligand, acetonitrile, was studied with hybrid QM/MM[22] metadynamics simulations[23,24] (see Computational Methods), where the Ni complex and the acetonitrile molecule coordinated to it were treated at the DFT level[25−27] and the rest of the acetonitrile solvent was described using an empirical potential.[28] The simulations indicated that the acetonitrile binding free energy is about 1.5 kcal/mol with an activation free energy for dissociation of about 5.8 kcal/mol (Figure S7 (Supporting Information)).

Chair/boat ring isomerization was studied with a standard stationary point search with a continuum description of the solvent. It was found that the activation barrier for the chair/boat transition of a six-membered ring depends on the configuration of the other ring on the same ligand. The concerted isomerization of two rings was found to have a considerably higher barrier (∼5 kcal/mol higher) than the stepwise isomerization of the two rings. Isomers with two rings of the same ligand in the same conformation (either chair or boat) are higher in free energy than isomers with the two rings in different conformations.

Using the network of reactions depicted in Figure 7, the rate for the acetonitrile exchange reaction was calculated according to a first-order kinetic model, as discussed previously.[7] In this

dx.doi.org/10.1021/om400695w | Organometallics 2013, 32, 7034−7042

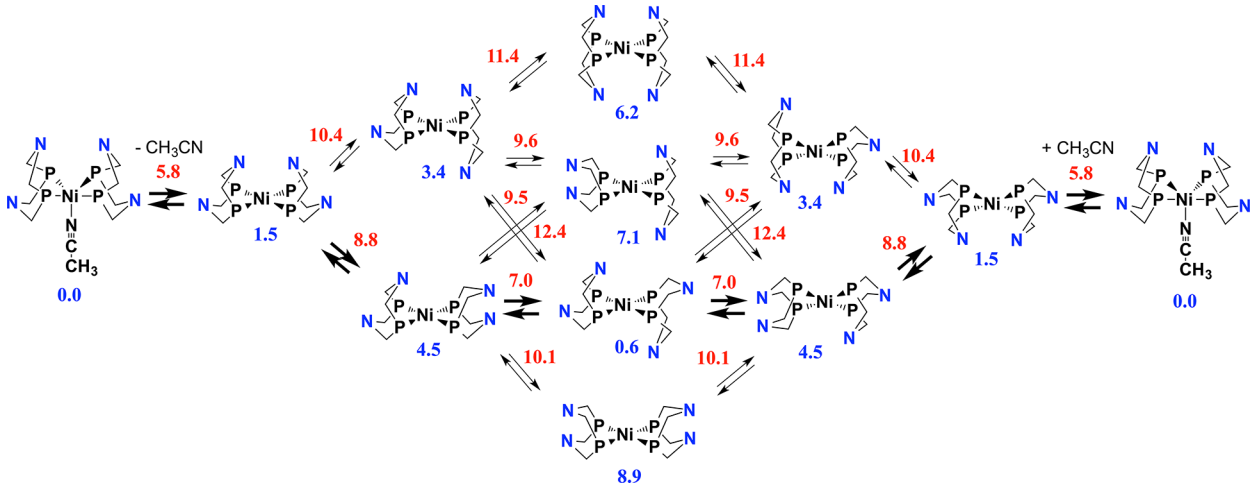

Figure 7. Possible pathways for the acetonitrile exchange reaction in $[Ni(CH_3CN)(P^{Ph}{}_2N^{Ph}{}_2)_2]^{2+}$. The most likely path is highlighted with bold arrows. The calculated free energies for the intermediates and activation free energies for each elementary step are reported in blue and red, respectively. All free energies are expressed in kcal/mol and are relative to the initial (or final) five-coordinate complex. Substituents on phosphorus and nitrogen are omitted for clarity. All complexes have a +2 charge that is not shown in the diagram.

calculation, acetonitrile association/dissociation was assumed to follow pseudo-first-order kinetics, $k' = k[CH_3CN]$, since acetonitrile is present in large excess. The kinetic model yielded an overall activation barrier for the exchange reaction of 8.9 kcal/mol at 25 °C, in excellent agreement with the experimentally observed activation barrier of 8.2 kcal/mol. Along any possible pathway, the chair/boat isomerization is rate-limiting. The most likely kinetic pathway is highlighted in Figure 7 using bold arrows. The pathway reported accounts for more than 98% of the overall reaction flow, on the basis of the calculated barriers for all of the possible pathways.

Dependence of Ring Isomerization on N Substituent. The overall dynamic process (Figures 6 and 7) includes chair/boat isomerization, which controls the positioning of the pendant amine. The boat conformation is necessary to position the proton relay endo to the metal to facilitate heterolytic cleavage of H_2 in H_2 oxidation catalysis or H−H bond formation in H_2 production catalysis. According to the calculations, the chair/boat isomerization is rate determining for the overall dynamic process observed for the $[Ni(P^R{}_2N^{R'}{}_2)_2]^{2+}$ complexes. Consistent with isomerization being rate-determining is the observation that a larger $\Delta G^{\ddagger}$ value was measured for $[Ni(P^{Ph}{}_2N^{tBu}{}_2)_2]^{2+}$ in comparison to $[Ni(P^{Ph}{}_2N^{Ph}{}_2)_2]^{2+}$ or $[Ni(P^{Cy}{}_2N^{Ph}{}_2)_2]^{2+}$. The nitrogen inversion is likely to be influenced by the sterics as well as the aromaticity of the nitrogen substituent;[29] therefore, the rate of chair/boat isomerization, i.e. the rate of proton relay positioning, can be affected by varying the substituents on the nitrogen.

To investigate this trend further, the rates of chair/boat isomerization were compared for complexes with different substituents at nitrogen for both Ni(0) complexes and Ni(II) hydrides. In these essentially tetrahedral complexes, two inequivalent ^{31}P resonances were observed at low temperature due to the asymmetry of the ^{31}P nuclei created by their proximity to a boat- or chair-positioned nitrogen of the opposite ligand. The interconversion of the ^{31}P occurs due to chair/boat isomerization.

For the zerovalent nickel complexes, $[Ni^0(P^{Cy}{}_2N^{Ph}{}_2)_2]$, $[Ni^0(P^{Cy}{}_2N^{Bn}{}_2)_2]$, and $[Ni^0(P^{Ph}{}_2N^{Bn}{}_2)_2]$ were compared. The corresponding temperature-dependent $^{31}P\{^1H\}$ spectra of the $[Ni^0(P^{Ph}{}_2N^{Bn}{}_2)_2]$ complex, shown in Figure 8, illustrate that the

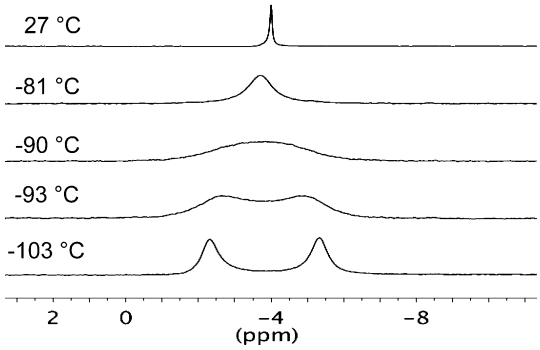

Figure 8. Variable-temperature $^{31}P\{^1H\}$ NMR spectra of $[Ni^0(P^{Ph}{}_2N^{Bn}{}_2)_2]$ in butyronitrile.

^{31}P resonances were observed to coalesce at approximately −90 °C. Line shape analysis was performed to obtain the activation parameters, as shown in Table 3 and the Eyring plot in Figure S5 (Supporting Information). The $\Delta G^{\ddagger}$ value of 6.5 kcal/mol is smaller than the $\Delta G^{\ddagger}$ = 7.7 kcal/mol[7] reported for $[Ni^0(P^{Cy}{}_2N^{Bn}{}_2)_2]$, which is consistent with theoretical calculations.[6] In $[Ni^0(P^{Cy}{}_2N^{Ph}{}_2)_2]$, however, the ^{31}P nuclei were still

Table 3. Comparison of $\Delta G^{\ddagger}$ Values for Isomerization of Nickel Complexes and Calculated $\Delta G^{\ddagger}$ Values for Inversion of Simple Amines in the Gas Phase

complex	$\Delta G^{\ddagger}$ (kcal/mol)
$[Ni(CH_3CN)(P^{Ph}{}_2N^{Ph}{}_2)_2]^{2+}$	8.2
$[Ni(CH_3CN)(P^{Ph}{}_2N^{tBu}{}_2)_2]^{2+}$	9.9
$[Ni(CH_3CN)(P^{Cy}{}_2N^{Ph}{}_2)_2]^{2+}$	7.9
$[Ni(H)(P^{Cy}{}_2N^{Ph}{}_2)_2]^{+}$	$\lesssim$5.5
$[Ni(H)(P^{Cy}{}_2N^{Bn}{}_2)_2]^{+}$	9.3[a]
$Ni(P^{Cy}{}_2N^{Ph}{}_2)_2$	$\lesssim$ 4.5
$Ni(P^{Cy}{}_2N^{Bn}{}_2)_2$	7.7[a]
$Ni(P^{Ph}{}_2N^{Bn}{}_2)_2$	6.5
$PhNH_2$	1.7[b]
NH_3	5.8[b]
NMe_3	6.0[b]

[a]Reference 7. [b]Reference 29.

dx.doi.org/10.1021/om400695w | Organometallics 2013, 32, 7034−7042

undergoing rapid exchange even at −105 °C, and only an average peak for the two ^{31}P nuclei was observed, as shown in Figure 9. The rapid exchange observed for $[Ni^0(P^{Cy}_2N^{Ph}_2)_2]$ is

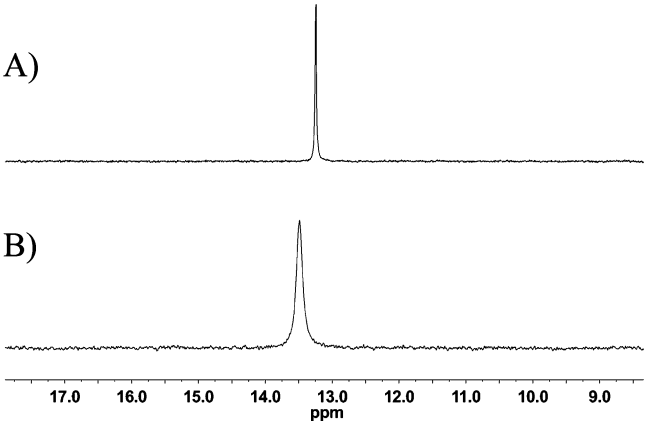

Figure 9. Variable-temperature $^{31}P\{^1H\}$ NMR spectra of $[Ni^0(P^{Cy}_2N^{Ph}_2)_2]$ at (A) 25 °C and (B) −105 °C in 1/1 THF/toluene.

indicative of a significantly smaller barrier for the chair/boat isomerization in this complex in comparison to the $[Ni^0(P^{Cy}_2N^{Bn}_2)_2]$ and $[Ni^0(P^{Ph}_2N^{Bn}_2)_2]$ complexes. The barrier could not be determined because the resonances still undergo rapid exchange at the low-temperature limit of the instrument. Therefore, the rate of ^{31}P exchange for the $[Ni^0(P^{Cy}_2N^{Ph}_2)_2]$ complex at −105 °C was estimated by assuming a similar difference in chemical shift for the ^{31}P resonances in comparison to the $[Ni^0(P^{Cy}_2N^{Bn}_2)_2]$ and $[Ni^0(P^{Ph}_2N^{Bn}_2)_2]$ complexes. This estimate gives a rate of 10000 s^{-1} at −105 °C and an upper limit of the $\Delta G^{\ddagger}$ value of approximately 4.8 kcal/mol.

For the Ni(II) hydride complexes, $[Ni(H)(P^{Cy}_2N^{Ph}_2)_2]^+$ and $[Ni(H)(P^{Cy}_2N^{Bn}_2)_2]^+$ were compared. The value of $\Delta G^{\ddagger}$ for $[Ni(H)(P^{Cy}_2N^{Bn}_2)_2]^+$ was reported previously as 9.3 kcal/mol.[7] The $[Ni(H)(P^{Cy}_2N^{Bn}_2)_2]^+$ complex exhibited coalescence of the ^{31}P NMR resonances at approximately −60 °C. The ^{31}P resonances of the $[Ni(H)(P^{Cy}_2N^{Ph}_2)_2]^+$ complex, on the other hand, were still undergoing rapid exchange at −105 °C (Figure 10). The rate of exchange for this complex at −105 °C was estimated, as it was for $[Ni(P^{Cy}_2N^{Ph}_2)_2]$ above, by assuming a similar difference in chemical shift for the ^{31}P resonances in

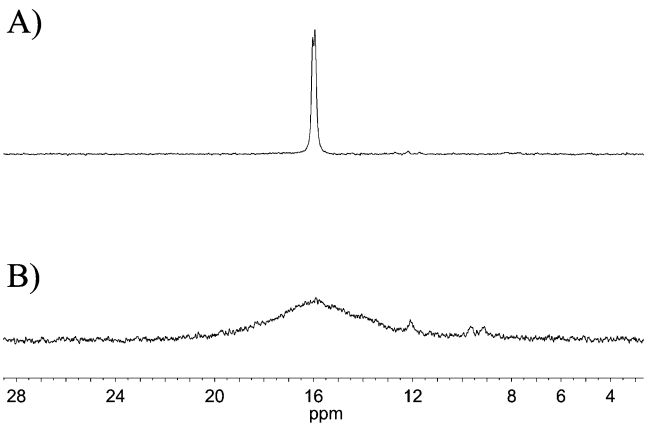

Figure 10. ^{31}P NMR spectra of $[Ni(H)(P^{Cy}_2N^{Ph}_2)_2]^+$ at (A) 25 °C and (B) −105 °C in butyronitrile.

comparison to $[Ni(H)(P^{Cy}_2N^{Bn}_2)_2]^+$. This estimation gives a rate of 1300 s^{-1} at −105 °C, which results in an upper limit of the $\Delta G^{\ddagger}$ value of 5.5 kcal/mol.

The $\Delta G^{\ddagger}$ value for chair/boat isomerization is the lowest for complexes with phenyl groups on the N atoms, regardless of the oxidation state or protonation state (Table 3). This observation is consistent with present and previous calculations,[6,7] which show that the activation barrier for the ring isomerization is lower for complexes with phenyl substituents on the pendant amine. For instance, the barrier for chair/boat isomerization in $[Ni(P^{Ph}_2N^{Ph}_2)_2]^{2+}$ is more than 2 kcal/mol smaller than the barrier calculated for $[Ni(P^{Cy}_2N^{Me}_2)_2]^{2+}$.[6] The reduced activation barrier is a consequence of the conjugation between the lone pair of the nitrogen atom and the π system of the phenyl ring. The conjugation is at a maximum at the transition state for the ring isomerization, resulting in a lower activation barrier for the aromatic substituents relative to the aliphatic substituents. This is a general trend for organic amines, where the $\Delta G^{\ddagger}$ value for nitrogen inversion of aniline is ∼4 kcal/mol lower than that of aliphatic amines such as trimethylamine.[29]

Mechanistic Implications of the Presence of the Fifth Ligand. The overall structural dynamic process, shown in Figures 6 and 7, includes the dissociation of a fifth ligand such as acetonitrile, which is a necessary step for H_2 oxidation catalysis. The five-coordinate $[Ni(CH_3CN)(P^R_2N^{R'}_2)_2]^{2+}$ species is not catalytically competent because the loss of acetonitrile is necessary to allow for H_2 binding in the hydrogen oxidation process. The dissociation of acetonitrile is very facile: i.e., an activation barrier of about 6 kcal/mol. This barrier is far smaller than the barrier for the heterolytic splitting of H_2 observed for our current H_2 oxidation catalysts (greater than 14 kcal/mol).[5,6] Therefore, dissociation of acetonitrile does not appear to be rate limiting. However, the five-coordinate complex is more stable than the catalytically competent four-coordinate species.[6] Consequently, the binding of acetonitrile can be detrimental to catalysis for the oxidation of H_2 because it results in the exergonic formation of a catalytically unproductive species.

The presence of a fifth ligand can also have important implications for hydrogen production, not on the rate but on the overpotential. While hydrogen production can start either with reduction of Ni(II) to Ni(I) or with protonation of the pendant amine, reduction prior to protonation occurs in the majority of the $[Ni(P^R_2N^{R'}_2)_2]^{2+}$ catalysts studied to date.[30,31] However, acetonitrile binds exclusively to the Ni(II) species and spontaneously dissociates upon reduction; in addition, its presence is not expected to influence protonation on the opposite face of the metal center.[6,8] Therefore, the fifth ligand is not expected to significantly impact the *kinetics* for H_2 production. However, its presence can shift the Ni(II/I) reduction potential toward more negative values and, consequently, can increase the overpotential associated with a given catalyst.[32] In the case of the $[Ni(P^{Ph}_2N^{Ph}_2)_2]^{2+}$ complex, a decrease of about 70 mV in the Ni(II/I) redox potential is predicted from quantum chemical calculations. The magnitude of the shift in the redox potential, and therefore the overpotential, depends on the nature of the phosphine ligands and nitrogen substituents.

SUMMARY AND CONCLUSIONS

The ligand structural dynamics have been characterized for a series of nickel complexes with $P^R_2N^{R'}_2$ ligands as a function of

dx.doi.org/10.1021/om400695w | *Organometallics* 2013, 32, 7034−7042

ligand identity, metal oxidation state, and protonation state. The dynamic structural exchange observed for $[Ni(P^R{}_2N^{R'}{}_2)_2]^{2+}$ complexes is proposed to occur through dissociation of a fifth ligand (CH_3CN or BF_4^-), boat/chair isomerization of each of the four rings (including nitrogen inversion), and reassociation of a fifth ligand on the opposite side of the complex. The dissociation of the fifth ligand is very facile, occurring with a barrier smaller than that for the overall exchange process, for which the chair/boat isomerization appears to be rate limiting. The chair/boat isomerization affects the positioning of the pendant amines, which need to be positioned endo to the metal (boat conformation) to either accept a proton during heterolytic cleavage of H_2 for catalytic oxidation of H_2 or deliver a proton to the metal hydride for catalytic production of H_2. The chair/boat isomerization process can be influenced by varying the substituent on the nitrogen atom, but the overall exchange process is fast relative to the maximum catalytic rates observed ($>10^4$ s^{-1} vs 10^3 s^{-1} at 25 °C), suggesting that these dynamic processes do not inhibit catalysis for the current $[Ni(P^R{}_2N^{R'}{}_2)_2]^{2+}$ catalysts.

The presence of a fifth ligand, however, can have significant implication for catalysis. Indeed, the five-coordinate complex is more stable than the catalytically active four-coordinate complex. Therefore, binding of a fifth ligand (for instance, the acetonitrile solvent) can slow down the catalytic oxidation of H_2, as it results in the formation of a stable, catalytically unproductive species. The presence of a fifth ligand coordinated to the Ni(II) center can also impact H_2 production catalysts because it makes the Ni(II)/Ni(I) reduction potential more negative, which increases the overpotential with respect to the four-coordinate Ni(II) complex.

MATERIALS AND METHODS

Materials and Instrumentation. Deuterated acetonitrile and toluene were dried by distillation from P_2O_5. Deuterated methylene chloride was dried by distillation from CaH_2. Dry solvents (not deuterated) were obtained using an Innovative Technologies Pure Solv solvent purification system. All other reagents were used as received from commercial sources. An LTQ Orbitrap Velos mass spectrometer (Thermo Scientific, San Jose, CA) outfitted with a custom electrospray ionization (ESI) interface was used for high-resolution mass spectroscopy experiments.

Synthesis of $P^{Ph}{}_2N^{tBu}{}_2$ Ligand. A 250 mL flask containing 150 mL of ethanol was charged with phenylphosphine (5.6 g, 50.80 mmol) and fresh paraformaldehyde (3.08 g, 102.5 mmol). The flask was heated at 75 °C in a hot oil bath, and the reaction mixture was stirred for 12 h, resulting in a clear solution. *tert*-Butylamine (3.72 g, 50.80 mmol) was added dropwise to the solution, and stirring was continued at 75 °C for another 12 h. The solution was filtered through a layer of Celite, and the solvent was removed with a vacuum. The resulting oily residue was dissolved in 3 mL of diethyl ether, and subsequently the ethereal solution was layered with 2 mL of CH_3CN. The solution was kept at −35 °C for 1 week to yield a slightly oily precipitate. Repeated purification of the precipitate by the same procedure led to a white powder product that was dried under vacuum (2.74 g, 26%). ^1H NMR (toluene-d_8): isomer a (56%), δ 3.64 (t, 4 H, J_{HH} = 10.0 Hz, NCH_2P), 3.32 (t, 4 H, J_{HH} = 10.0 Hz, NCH_2P), 1.02 (s, 18 H, ^{t}BuP); isomer b (44%), δ 3.75 (dd, 4 H, J_{HH} = 10.0 Hz, J_{PH} = 5.0 Hz, NCH_2P), 3.17 (dd, 4 H, J_{HH} = 10.0 Hz, J_{PH} = 5.0 Hz, NCH_2P), 1.07 (s, 18 H, ^{t}BuP). The proton resonances of the phenyl groups (from 6.98 to 7.68 ppm) for both isomers are overlapped and cannot be distinguished. ^{31}P NMR ($CDCl_3$): isomer a (56%), δ −25.84 (s); isomer b (44%), δ −27.33 (s). Obtaining a satisfactory combustion analysis has proven to be difficult for this new compound, as the carbon analysis is repeatedly low. ESI exact mass spectroscopy data and ^1H, ^{13}C, and ^{31}P NMR spectra are provided to address compound identity and purity. ESI mass spectroscopy data, m/z^+: $C_{24}H_{37}N_2P_2$ calcd (found) 415.2432 (415.2431). See Figures S8−S10 (Supporting Information) for ^1H, $^{13}C\{^1H\}$, and $^{31}P\{^1H\}$ NMR spectra.

Synthesis of Ni Complexes. Recently reported procedures were followed for the synthesis of $[Ni(H)(P^{Cy}{}_2N^{Ph}{}_2)_2][BF_4]$, $[Ni(P^{Ph}{}_2N^{Bn}{}_2)_2][BF_4]_2$, $[Ni(P^{Ph}{}_2N^{Bn}{}_2)_2]$, and $[Ni(P^{Ph}{}_2N^{Ph}{}_2)_2][BF_4]_2$.[12,15,30,33] The spectral properties are consistent with those previously reported.

$[Ni(P^{Ph}{}_2N^{tBu}{}_2)_2][BF_4]_2$ was synthesized by adding a slurry of $[Ni(CH_3CN)_6][BF_4]_2$ (48 mg, 0.1 mmol) to a solution of $P^{Ph}{}_2N^{tBu}{}_2$ (76 mg, 0.18 mmol) in 5 mL of CH_2Cl_2. The red solution was stirred overnight and filtered and the solvent removed by vacuum. The orange solid was washed with hexane (yield 80 mg, 79%). ^1H NMR (20% (v/v) CD_3CN/CD_2Cl_2): 1.26 ($NC(CH_3)_3$, s, 36H), 3.28 (PCH_2N, d, J_{HH} = 13 Hz, 8.21H), 3.83 (PCH_2N, dd, J_{HH} = 13 Hz, J_{P-H} = 4 Hz, 8.40 H), 7.17−7.25 ($P(C_6H_5)$, m, 13.79 H) 7.44 ($P(C_6H_5)$, m, 5.41 H). $^{13}C\{^1H\}$ NMR (20% (v/v) CD_3CN/CD_2Cl_2): 26.4 ($NC(CH_3)_3$); 58.3 (PCH_2N); 129.6, 130.0, 131.5 ($P(C_6H_5)$, m, 4.31 H). $^{31}P\{^1H\}$ NMR (20% v/v CD_3CN/CD_2Cl_2): 4.72 (s). Obtaining a satisfactory combustion analysis has proven to be difficult for this new complex, as the carbon analysis is repeatedly low. ESI exact mass spectroscopy data and ^1H, ^{13}C, and ^{31}P NMR spectra are provided to address compound identity and purity. ESI mass spectroscopy data, m/z^+ for the dication: $C_{48}H_{72}N_4NiP_4$ calcd (found) 443.2025 (443.2039). See Figures S11−S13 (Supporting Information) for ^1H, $^{13}C\{^1H\}$, and $^{31}P\{^1H\}$ NMR spectra.

$[Ni(Cl)(P^{Ph}{}_2N^{Ph}{}_2)_2][BF_4]$ was synthesized by adding 2 equiv (4 mg, 0.08 mmol) of NH_4Cl to an acetonitrile solution of $[Ni(P^{Ph}{}_2N^{Ph}{}_2)_2][BF_4]_2$ (50 mg, 0.04 mmol). After it was stirred overnight, the solution turned from pink to dark purple. The solution was then filtered and the solvent removed to give a purple solid (yield 27 mg, 56%). Exact ESI mass spectroscopy: m/z^+ $C_{56}H_{56}ClN_4NiP_4$ calcd (found) 1001.2492 (1001.2633). X-ray-quality dark purple rectangular crystals were obtained from diffusion of diethyl ether into an acetonitrile solution. See Figures S3 and S4 and Table S1 (Supporting Information) for the $^1H-^{13}C$ HSQC spectrum, crystallographic data, and resonance assignments.

$[Ni^0(P^{Cy}{}_2N^{Ph}{}_2)_2]$ was synthesized in situ by combining commercially obtained Ni(cyclooctadiene)$_2$ (6 mg, 0.03) with 2 molar equiv of $P^{Cy}{}_2N^{Ph}{}_2$ (23 mg, 0.05 mmol) in 1.5 mL of 1/1 (v/v) THF/toluene. ^1H NMR (d_8-THF/d_8-toluene): 1.22−1.77 ((C_6H_{11}, m), 3.38−3.47 (PCH_2N, m), 6.82−7.21 ($P(C_6H_5)$, m). ^{31}P $\{^1H\}$ NMR (d_8-THF/d_8-toluene): 10.7 (s). Exact ESI mass spectroscopy: m/z^+ $C_{56}H_{81}N_4NiP_4$ calcd (found) 991.4760 (991.4756).

X-ray quality yellow block crystals of $[Ni(P^{Ph}{}_2N^{Bn}{}_2)_2]$ were grown by slow evaporation of the THF solution at room temperature. See Figure S14 for crystallographic data.

NMR Studies. A 500 MHz ^1H frequency Agilent VNMRS or Inova system (Palo Alto, CA) equipped with a direct detect dual band probe was used for all studies. Typical 90° pulses were ∼8 μs for ^1H and ∼12 μs for ^{31}P. $^{31}P\{^1H\}$ NMR spectra were collected with WALTZ decoupling. The temperature was controlled from −105 to +50 °C using an XRII852 Sample Cooler (FTS Systems, Stone Ridge, NY) FTS chiller system or liquid nitrogen. 2D HSQC, HMBC, COSY, and TOCSY pulse sequences were used from the VNMRJ 3.1 software suite.

NMR Spectroscopy Sample Preparation. NMR samples were prepared by dissolving ∼10 mg of complex in 0.4 mL of deuterated solvent. A 0.1 mL portion of acetonitrile was added by syringe to result in ∼15 mM solutions.

NMR Line Shape Analysis. The gNMR program was used for analysis of the exchange processes observed in the variable-temperature ^1H and ^{31}P spectra. gNMR was used to process NMR spectra using a Lorentzian function with up to 6 Hz line broadening. A two-site exchange model was used to determine the rates of nuclei exchange by iteration of the simulated line widths, using both manual and gNMR algorithm methods.[16−18] See Figure S1 (Supporting Information) for representative spectra and simulations.

Kinetic Analysis. Eyring parameters were determined using eq 1, relating rate as a function of temperature. Individual error bars of 7−15% were applied to the exchange rate determined at a given temperature. The error bars were estimated manually on the basis of visual inspection of the overlaid experimental and simulated spectrum from gNMR; see Figure S2 (Supporting Information) for representative spectra. Profit software was used for data analysis, where the nonlinear regression was done with the 7−15% errors applied to the individual data points. The temperature of the NMR spectrometer was calibrated using a methanol standard, and the error in the temperature was estimated to be 0.5 K. The error in the activation parameters were determined by the error propagation method described by Girolami et al.[34]

$$k = \frac{k_B T}{h} e^{\Delta H^{\ddagger}/RT} e^{\Delta S^{\ddagger}/R} \quad (1)$$

X-ray Crystallography. A Bruker-AXS Kappa Apex II CCD diffractometer with 0.71073 Å Mo Kα radiation was used for data collection. Crystals were mounted on a MiTeGen MicroMounts pin using Paratone-N oil. Data were collected at 100 K. The software used for data analysis includes Brüker APEX II software[35] to retrieve cell parameters and SAINTPlus[36] for raw data integration, and absorption correction was applied using SADABS.[37] The structures were solved using either direct methods or the Patterson method and refined by a least-squares method on F^2 using the SHELXTL program package. Space groups were chosen by analysis of systematic absences and intensity statistics.[38]

Computational Methods. The kinetic model reported in Figure 8 was elaborated by employing two different computational schemes. (1) Hybrid quantum mechanics/molecular mechanics (QM/MM) molecular dynamics (MD) simulations were carried out to calculate acetonitrile association and dissociation free energies. (2) Quantum chemical optimizations of stationary points with a continuum description of the solvent were used instead to study chair/boat inversions. A detailed discussion of the adopted approach was reported in previous publications.[6,8]

Calculation of the Acetonitrile Binding Free Energy. The MD simulations were carried out on the $[Ni(CH_3CN)(P^{Ph}{}_2N^{Ph}{}_2)_2]^{2+}$ complex using the following procedure. The Ni complex was embedded in 1032 acetonitrile molecules in a cubic box size of 48.44 Å × 48.44 Å × 48.44 Å. The system was equilibrated for 2 ns at constant pressure[39] and constant temperature[40] using a force field description,[28] keeping the Ni catalyst frozen in its gas-phase optimized structure (see the first structure in Figure 7). The protocol adopted for these simulations was described in a previous publication.[6] One configuration with an acetonitrile molecule bound to the metal center was extracted from the resulting trajectory and used as the initial configuration in all subsequent QM/MM calculations. In the QM/MM calculations, the Ni complex and the bound acetonitrile molecule were treated at the QM level of theory. The electrostatic interactions between the QM and MM subsystems were described by a real space, multigrid, linear scaling coupling scheme.[22] The system was then relaxed at the QM/MM level of theory and equilibrated at constant volume and constant temperature for about 2 ps using an integration time step of 0.25 fs. The QM/MM simulation was carried out within the DFT framework using the hybrid Gaussian and plane waves (GPW) method implemented in the CP2K code.[41] A triple-ζ basis set augmented with two sets of d-type and p-type polarization functions was employed for the valence electrons of all the atoms (TZV2P basis set).[42] The interaction between valence and core electrons was described using norm-conserving pseudopotentials.[43] The electrostatic energy was calculated using an auxiliary plane wave basis set with a cutoff energy of 280 Ry in a 27 × 27 × 27 Å^3 periodic cubic box. The Perdew−Burke−Ernzerhof (PBE) exchange and correlation functional[25,26] was employed along with Grimme's correction for dispersion interactions (PBE+D).[27] Previous calculations showed that the PBE+D level of theory yields good descriptions of the energetics associated with the $[Ni(P^R{}_2N^{R'}{}_2)_2]^{2+}$ catalysts and gives results comparable to those obtained with the more accurate hybrid B3P86 functional[6] used for the exploration of the conformational space (see below). The metadynamics technique[23,24] was employed to obtain the free energy profile for the dissociation and association of acetonitrile by using the distance between the metal center and the N atom of the acetonitrile molecule. This distance was biased adding Gaussian functions of 0.1 kcal/mol height and 0.1 Å width every 20 fs. The simulation was run for 25 ps. Simulations were carried out with the CP2K program.

Exploration of the Isomer Space and Calculation of the Chair/Boat Inversion Barriers. Structures of all of the possible conformers were optimized using molecular DFT calculations with the B3P86 hybrid functional[44,45] along with the Stuttgart−Dresden relativistic effective core potential and associated basis set (SDD) for Ni[46] and 6-31G* for all nonmetal atoms with additional p polarization function on the H_2 molecule.[47,48] Harmonic vibrational frequencies were calculated for the optimized structures using the same level of theory to estimate the zero-point energy (ZPE) and thermal contributions (T = 298 K and P = 1 bar) to the gas-phase free energy. Solvation free energies were then computed using a self-consistent reaction field model at the same level of theory as for the other steps. The continuum polarizable conductor model[49,50] was used with Bondi radii.[51] These calculations were carried out with Gaussian 09.[52]

■ ASSOCIATED CONTENT

Supporting Information

Figures, tables, text, and CIF files giving experimental and simulated NMR spectra, details of the X-ray structures, additional computation details, and the full citation for ref 52. This material is available free of charge via the Internet at http://pubs.acs.org.

■ AUTHOR INFORMATION

Corresponding Authors

*E-mail for A.M.A.: aaron.appel@pnnl.gov.
*E-mail for S.R.: simone.raugei@pnnl.gov.

Notes

The authors declare no competing financial interest.

■ ACKNOWLEDGMENTS

We dedicate this paper to the memory of Dr. James A. Franz (1948−2010): a great scientist, mentor, and friend. Research by J.A.F., M.O., M.-H.H., M.L.H., D.L.D., A.M.A., S.R., and R.M.B. was supported as part of the Center for Molecular Electrocatalysis, an Energy Frontier Research Center funded by the U.S. Department of Energy, Office of Science. W.J.S. and S.L. were funded by the DOE Office of Science Early Career Research Program through the Office of Basic Energy Sciences. T.L. was supported by the U.S. Department of Energy, Office of Basic Energy Sciences, Division of Chemical Sciences, Geosciences & Biosciences. Pacific Northwest National Laboratory (PNNL) is a multiprogram national laboratory operated for the DOE by Battelle. Computational resources were provided at W. R. Wiley Environmental Molecular Science Laboratory (EMSL), a national scientific user facility sponsored by the Department of Energy's Office of Biological and Environmental Research located at Pacific Northwest National Laboratory, the National Energy Research Scientific Computing Center (NERSC) at Lawrence Berkeley National Laboratory, and the Jaguar supercomputer at Oak Ridge National Laboratory (INCITE 2008−2011 award supported by the Office of Science of the U.S. DOE under Contract No. DE-AC0500OR22725).

REFERENCES

(1) Nicolet, Y.; de Lacey, A. L.; Vernède, X.; Fernandez, V. M.; Hatchikian, E. C.; Fontecilla-Camps, J. C. *J. Am. Chem. Soc.* **2001**, *123*, 1596−1601.
(2) DuBois, D. L.; Bullock, R. M. *Eur. J. Inorg. Chem.* **2011**, 1017−1027.
(3) Helm, M. L.; Stewart, M. P.; Bullock, R. M.; DuBois-Rakowski, M.; DuBois, D. L. *Science* **2011**, *333*, 863−866.
(4) Yang, J. Y.; Smith, S. E.; Liu, T.; Dougherty, W. G.; Hoffert, W. A.; Kassel, W. S.; DuBois-Rakowski, M.; DuBois, D. L.; Bullock, R. M. *J. Am. Chem. Soc.* **2013**, *135*, 9700−9712.
(5) Yang, J. Y.; Chen, S.; Dougherty, W. G.; Kassel, W. S.; Bullock, R. M.; DuBois, D. L.; Raugei, S.; Rousseau, R.; Dupuis, M.; Rakowski DuBois, M. *Chem. Commun.* **2010**, *46*, 8618−8620.
(6) Raugei, S.; Chen, S.; Ho, M.-H.; Ginovska-Pangovska, B.; Rousseau, R. J.; Dupuis, M.; DuBois, D. L.; Bullock, R. M. *Chem. Eur. J.* **2012**, *18*, 6493−6506.
(7) O'Hagan, M.; Shaw, W. J.; Raugei, S.; Chen, S.; Yang, J. Y.; Kilgore, U. J.; DuBois, D. L.; Bullock, R. M. *J. Am. Chem. Soc.* **2011**, *133*, 14301−14312.
(8) O'Hagan, M.; Ho, M.-H.; Yang, J. Y.; Appel, A. M.; DuBois-Rakowski, M.; Raugei, S.; Shaw, W. J.; DuBois, D. L.; Bullock, R. M. *J. Am. Chem. Soc.* **2012**, *134*, 19409−19424.
(9) Kilgore, U.; Roberts, J.; Pool, D. H.; Appel, A.; Stewart, M.; Rakowski DuBois, M.; Dougherty, W. G.; Kassel, W. S.; Bullock, R. M.; DuBois, D. L. *J. Am. Chem. Soc.* **2011**, *133*, 5861−5872.
(10) Kilgore, U. J.; Stewart, M. P.; Helm, M. L.; Dougherty, W. G.; Kassel, W. S.; DuBois-Rakowski, M.; DuBois, D. L.; Bullock, R. M. *Inorg. Chem.* **2011**, *50*, 10908−10918.
(11) Miedaner, A.; Haltiwanger, R. C.; DuBois, D. L. *Inorg. Chem.* **1991**, *30*, 417−427.
(12) Galan, B. R.; Schöffel, J.; Linehan, J. C.; Seu, C.; Appel, A. M.; Roberts, J. A. S.; Helm, M. L.; Kilgore, U. J.; Yang, J. Y.; DuBois, D. L.; Kubiak, C. P. *J. Am. Chem. Soc.* **2011**, *133*, 12767−12779.
(13) Seu, C. S.; Appel, A. M.; Doud, M. D.; DuBois, D. L.; Kubiak, C. P. *Energy Environ. Sci.* **2012**, *5*, 6480−6490.
(14) Wiese, S.; Kilgore, U. J.; DuBois, D. L.; Bullock, R. M. *ACS Catal.* **2012**, *2*, 720−727.
(15) Wilson, A. D.; Newell, R. H.; McNevin, M. J.; Muckerman, J. T.; Rakowski DuBois, M.; DuBois, D. L. *J. Am. Chem. Soc.* **2006**, *128*, 358−366.
(16) Budzelaar, P. H. M. *gNMR 5.0*; IvorySoft, 1995−2006.
(17) Binsch, G. In *Dynamic Nuclear Magnetic Resonance Spectroscopy*; Jackman, L. M., Cotton, F. A., Eds.; Academic: London, 1975.
(18) Steigel, A. *NMR, Basic Principles and Progress*; Diehl, P. F., Fluck, E., Kosfeld, R., Eds.; Springer-Verlag: Berlin, 1978; Vol. *15*, p 1.
(19) Berry, R. S. *J. Chem. Phys.* **1960**, *32*, 933−938.
(20) Honeychuck, R. V.; Hersh, W. H. *Inorg. Chem.* **1989**, *28*, 2869−2886.
(21) Cheng, T.-Y.; Szalda, D. J.; Franz, J. A.; Bullock, M. R. *Inorg. Chim. Acta* **2010**, *363*, 581−585.
(22) Laino, T.; Mohamed, F.; Laio, A.; Parrinello, M. *J. Chem. Theory Comput.* **2006**, *2*, 1370−1378.
(23) Laio, A.; Gervasio, F. L. *Rep. Prog. Phys.* **2008**, *71*, 126601.
(24) Laio, A.; Parrinello, M. *Proc. Natl. Acad. Sci. U.S.A.* **2002**, *99*, 12562−12566.
(25) Perdew, J. P.; Burke, K.; Ernzerhof, M. *Phys. Rev. Lett.* **1997**, *78*, 1396−1396.
(26) Perdew, J. P.; Burke, K.; Ernzerhof, M. *Phys. Rev. Lett.* **1996**, *77*, 3865−3868.
(27) Grimme, S. *J. Comput. Chem.* **2006**, *27*, 1787−1799.
(28) Nikitin, A. M.; Lyubartsev, A. P. *J. Comput. Chem.* **2007**, *28*, 2020−2026.
(29) Rauk, A.; Andose, J. D.; Frick, W. G.; Tang, R.; Mislow, K. *J. Am. Chem. Soc.* **1971**, *93*, 6507−6515.
(30) Appel, A. M.; Pool, D. H.; O'Hagan, M.; Shaw, W. J.; Yang, J. Y.; Rakowski DuBois, M.; DuBois, D. L.; Bullock, R. M. *ACS Catal.* **2011**, *1*, 777−785.
(31) Pool, D. H.; Stewart, M. P.; O'Hagan, M.; Shaw, W. J.; Roberts, J. A. S.; Bullock, R. M.; DuBois, D. L. *Proc. Natl. Acad. Sci. U.S.A.* **2012**, *109*, 15634−15639.
(32) Horvath, S.; Fernandez, L. E.; Appel, A. M.; Hammes-Schiffer, S. *Inorg. Chem.* **2013**, *52*, 3643−3652.
(33) Fraze, K.; Wilson, A. D.; Appel, A. M.; Rakowski DuBois, M.; DuBois, D. L. *Organometallics* **2007**, *26*, 3918−3924.
(34) Morse, P. M.; Spencer, M. D.; Wilson, S. R.; Girolami, G. S. *Organometallics* **1994**, *13*, 1646−1655.
(35) *APEX II, 2010.3-0*; Bruker AXS Inc., Madison, WI, 2009.
(36) *SAINTPlus*; Bruker AXS Inc., Madison, WI, 2004.
(37) *SADABS*; Bruker AXS Inc., Madison, WI, 2001.
(38) Sheldrick, G. M. *SHELXTL 6.14*; Bruker AXS Inc., Madison, WI, 2004.
(39) Parrinello, M.; Rahman, A. *J. Appl. Phys.* **1981**, *52*, 7182−7190.
(40) Martyna, G. J.; Klein, M. L.; Tuckerman, M. *J. Chem. Phys.* **1992**, *97*, 2635−2643.
(41) VandeVondele, J.; Krack, M.; Mohamed, F.; Parrinello, M.; Chassaing, T.; Hutter, J. *Comput. Phys. Commun.* **2005**, *167*, 103−128.
(42) VandeVondele, J.; Hutter, J. *J. Chem. Phys.* **2007**, *127*, 114105−114109.
(43) Goedecker, S.; Teter, M.; Hutter, J. *Phys. Rev. B* **1996**, *54*, 1703−1710.
(44) Perdew, J. P. *Phys. Rev. B: Condens. Matter* **1986**, *33*, 8822−8824.
(45) Becke, A. D. *J. Chem. Phys.* **1993**, *98*, 5648−5652.
(46) Andrae, D.; Häußermann, U.; Dolg, M.; Stoll, H.; Preuß, H. *Theor. Chem. Acc.* **1990**, *77*, 123−141.
(47) Rassolov, V. A.; Pople, J. A.; Ratner, M. A.; Windus, T. L. *J. Chem. Phys.* **1998**, *109*, 1223−1229.
(48) Chen, S.; Raugei, S.; Rousseau, R.; Dupuis, M.; Bullock, R. M. *J. Phys. Chem. A* **2010**, *114*, 12716−12724.
(49) Cossi, M.; Rega, N.; Scalmani, G.; Barone, V. *J. Comput. Chem.* **2003**, *24*, 669−681.
(50) Barone, V.; Cossi, M. *J. Phys. Chem. A* **1998**, *102*, 1995−2001.
(51) Bondi, A. *J. Phys. Chem.* **1964**, *68*, 441−451.
(52) Frisch, M. J., et al. *Gaussian 03, Revision D.02*; Gaussian, Inc., Wallingford, CT, 2004.